

A Coin Vibrational Motor Swimming at Low Reynolds Number

Alice C. Quillen^{1*}, Hesam Askari^{2**}, Douglas H. Kelley^{2***},
Tamar Friedmann^{1,3,4****}, and Patrick W. Oakes^{1*****}

¹Dept. of Physics and Astronomy, University of Rochester, Rochester, NY, 14627, USA

²Dept. of Mechanical Engineering, University of Rochester, Rochester, NY, 14627, USA

³Dept. of Mathematics, University of Rochester, Rochester, NY, 14627, USA

⁴Dept. of Mathematics and Statistics, Smith College, Northampton, MA, 01063, USA

Received August 30, 2016; accepted December 10, 2016

Abstract—Low-cost coin vibrational motors, used in haptic feedback, exhibit rotational internal motion inside a rigid case. Because the motor case motion exhibits rotational symmetry, when placed into a fluid such as glycerin, the motor does not swim even though its oscillatory motions induce steady streaming in the fluid. However, a piece of rubber foam stuck to the curved case and giving the motor neutral buoyancy also breaks the rotational symmetry allowing it to swim. We measured a 1 cm diameter coin vibrational motor swimming in glycerin at a speed of a body length in 3 seconds or at 3 mm/s. The swim speed puts the vibrational motor in a low Reynolds number regime similar to bacterial motility, but because of the oscillations of the motor it is not analogous to biological organisms. Rather the swimming vibrational motor may inspire small inexpensive robotic swimmers that are robust as they contain no external moving parts. A time dependent Stokes equation planar sheet model suggests that the swim speed depends on a steady streaming velocity $V_{stream} \sim Re_s^{1/2} U_0$ where U_0 is the velocity of surface oscillations, and streaming Reynolds number $Re_s = U_0^2 / (\omega \nu)$ for motor angular frequency ω and fluid kinematic viscosity ν .

MSC2010 numbers: 76D07, 76D99, 76Z99, 74F99, 74L99, 74H99, 70B15, 68T40, 35Q99

DOI: 10.1134/S1560354716070121

Keywords: swimming models, hydrodynamics, nonstationary 3-D Stokes equation, bio-inspired micro-swimming devices

1. INTRODUCTION

Locomotion mechanisms of small biological organisms can inspire strategies for achieving efficient locomotion in small artificial or robotic mechanisms. Alternatively new construction principles can be invented that might be simpler, more efficient or practical from an engineering perspective. Self-propulsion forces arise from the mechanical dissipative interactions of the organism or locomotor with a surrounding fluid, granular material or with a solid substrate (e.g., [2, 6, 11, 16, 22–24]). Small or microscopic synthetic swimmers could be valuable in diverse fields. For example, robotic swimmers could transport cargo, e.g., in medicine or microfluidic chips, or locate and process toxic materials in the environment.

A series of motions of minimal complexity that can give a net body displacement often involves periodic shape changes. At low Reynolds number in a fluid, locomotion is not possible if the body can only deform with one degree of freedom. The Navier–Stokes equation in this limit

*E-mail: alice.quillen@rochester.edu

**E-mail: askari@rochester.edu

***E-mail: d.h.kelley@rochester.edu

****E-mail: tfriedmann@smith.edu

*****E-mail: poakes@rochester.edu

is time independent and so trajectories (in the space of body shapes) that are time reversible return the body to its original shape, orientation and position [33]. This implies that a scallop or clam cannot swim by open and closing its shell and that additional degrees of freedom are required for locomotion. This rule is known as Purcell's "scallop theorem" [22, 33]. After a cyclical sequence of body deformations that returns the body to its original shape (a gait or a swimming stroke), the body translation and rotation depends quadratically on the amplitude of the deformations [9, 25, 40, 43]. Transformations of the body shape are elements of a symmetry group that is embedded in a larger manifold that includes body translations and rotations. In this sense swimming at low Reynolds number can be considered a gauge theory [40]. In the language of differential geometry, locomotion is only possible if the infinitesimal generators of deformations do not commute [33, 40]. Constraints on the body arising from its interaction with the external world give rise to a *connection* on the principal bundle of shapes and the holonomy of a closed loop in body shape space give rise to the net motion of a swimming stroke.

Appendages such as cilia and flagella present both manufacturing and operational challenges for microscopic robots [15]. They could break, fall off, get stuck or damage tissues. Some bacteria swim without flagella or cilia, due to traveling wave-like deformations along their cell surfaces [9, 10, 14]. Spirochetes generate thrust by rotating long helical flagella. However, spirochete flagella are internal, residing within the space between the inner and outer membranes and the flagella are never in direct contact with the external fluid [14]. Because they swim without cilia or flagella, spirochetes could inspire strategies for robotic swimming without appendages at low Reynolds number.

At low Reynolds number, the Navier–Stokes equation becomes $\mu \nabla^2 \mathbf{u} = \nabla p$, (the Stokes equation) with p the pressure, μ the viscosity and \mathbf{u} the velocity. The Stokes equation combined with a condition for an incompressibility $\nabla \cdot \mathbf{u} = 0$ is known as Stokes flow. One can solve this elliptic partial differential equation (see [41]), 1) with any choice of boundary velocities that produce the instantaneous change of shape, 2) by subtracting an appropriate instantaneous, infinitesimal rigid motion counter flow so that the net force and torque on the body from the combined flows vanish. There is a related connection between the locomotion of a body due to oscillatory motion and the locomotion of a body due to oscillations in the fluid. [46] proposed that a vibrating dumbbell micro-bot, comprised of two spheres of different density separated by a vibrating actuator, could swim in a viscous fluid. [20] later showed experimentally that two unequal density spheres connected with a spring swam when placed in a vibrating viscous fluid. [28] explored propulsion of a nearly round particle that is floating in a vibrating fluid. Swim velocities, motivated by biological organisms, have primarily been estimated for Stokes flow (e.g., [9]), though [18] studied control of a system of connected parts using the time dependent or non-stationary Stokes flow equation; $\rho \frac{\partial \mathbf{u}}{\partial t} = -\nabla p + \mu \nabla^2 \mathbf{u}$, with ρ the fluid density.

A simple and inexpensive vibrational swimmer would provide opportunities to explore experimentally the hydrodynamics of locomotion for oscillating and vibrating mechanisms. Such a mechanism would aid or inspire development of small and robust robotic swimmers.

In this paper we present a novel and low-cost swimmer constructed from a coin vibrational motor. In Section 2 we describe the internal rotational motion of a coin vibrational motor and the construction of a swimmer. Using a movie of the swimmer (see <https://youtu.be/0nP2Mgza0yU>) in Section 2.1 we measure the swim speed in glycerin and tabulate dimensionless parameters describing the hydrodynamics regime. In Section 2.2 particle trajectories are used to illustrate and measure induced fluid motions. Internal oscillations of the vibrational motor cause periodic motions of the rigid motor case and this induces steady streaming in the fluid. The streaming motions are predominantly rotational about the motor. To swim, the rotational symmetry of the mechanism and associated flow must be broken, and this is achieved with a piece of foam rubber that also maintains neutral buoyancy and prevents the motor case from rotating. Within the context of the physical quantities measured from our movie, in Section 3 we discuss the hydrodynamics. In Section 3.1 we modify the planar sheet model by [43]. Using the time-dependent Stokes equation we compute the steady streaming velocity induced by the oscillatory motion of a rigid planar sheet. This and a rough application of the tangent plane approximation gives us an estimate for the motor swim velocity and provides an explanation for why the vibrational motor swims. A summary and discussion follows in Section 4.

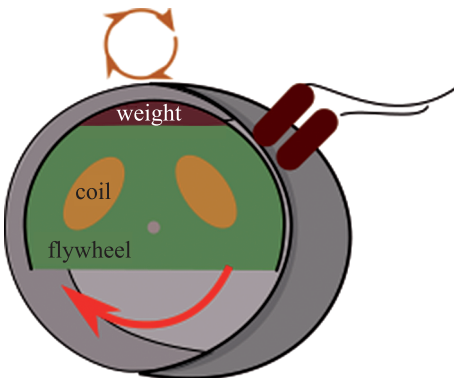


Fig. 1. An illustration of a coin vibrational motor. The motor case is rigid and we assume that its rotation is prevented. A lopsided flywheel inside rotates causing the entire case to move in a circle in a direction counteracting the motion of the internal weight. Each point on the surface of the case moves in a circle, here shown with a brown circle with arrows. The case surface translates first downwards, then to the left, then upwards, and then to the right (or vice versa if the flywheel inside the motor rotates in the opposite direction).

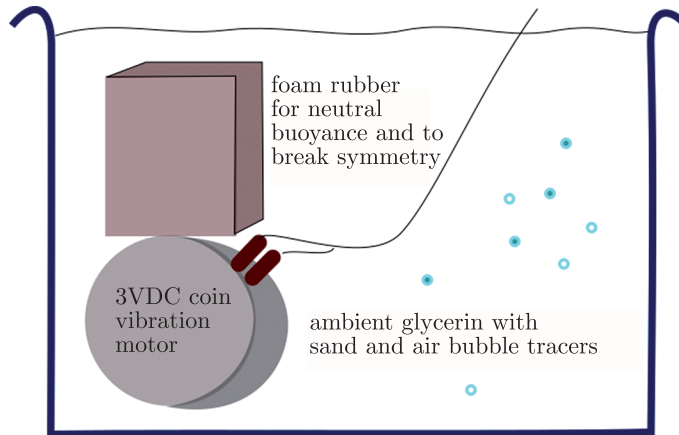


Fig. 2. An illustration of a swimming vibrational motor. Foam rubber is used to make the swimmer neutrally buoyant and break rotational symmetry. The actual container used is much larger than the one illustrated here, relative to the size of the motor.

2. A VIBRATIONAL MOTOR SWIMMER

Slim and compact coin vibrational motors are cheap and ubiquitous because of their use in cell phones and pagers. Electric rotating mass (ERM) vibrational motors vibrate because they contain a lopsided internal flywheel that rotates, at typically between 10000 and 12000 rpm; see Fig. 1 for an illustration. As the moving object is internal to the case, vibrational motors provide a novel and low-cost realization of the robotic swimmer concepts proposed and investigated by [6, 9, 44, 45], who considered locomotion in fluid of an idealized body containing an internal mass that moves within the body (also see [36]). Locomotion due to motions internal to the body at the cellular level was investigated by [12]. A bacterial analog might be the spirochete where the rotating flagella lie beneath an outer cellular membrane, though there the internal motion causes deformation of the outer membrane and the body is approximately incompressible. In contrast, the case of the vibrational motor is rigid but the mass density inside is not homogeneous.

We use a 3VDC coin vibrational motor (digikey part number 1597-1244-ND, manufacturer Seeed Technology, manufacturer part number 316040001, price \$1.20) with diameter 10 mm and width 2.5 mm. The internal flywheel is specified to run at least at 10000 rpm (according to the specification sheet provided by the manufacturer) corresponding to a frequency of 167 Hz and an angular frequency of $\omega = 1050 \text{ s}^{-1}$. The frequency, 167 Hz, is barely audible but ideal for haptic feedback.

We powered the motor with a table top regulated DC power supply. The power is connected to the motor with 42 AWG polyurethane coated magnet wire (0.064 mm diameter). Fine wire was chosen so as to minimize drag from the power wires as they move through the fluid.

In free space, the geometric center of the case would traverse a circle centered on the system's center of mass, and rotating in a direction opposite to that of the lopsided flywheel. However, the foam rubber and power wires stop the rigid motor case from counter-rotation but not from moving altogether. Each point on the case surface moves in a small loop (see Fig. 1; assuming that the case is not rotating). A rotation period consists of first moving upward, then to the right, then downward then to the left and then back to the original position (or vice versa if the flywheel rotates in the opposite direction). Each point on the case surface executes the same motion simultaneously. Taking a cylindrical coordinate system with origin at the center of mass, we consider a moment when the case is moving upward. At that time, the direction of motion is normal to the surface at a point on the top of the case, normal to the surface but in the opposite direction at a point on the bottom of the case. However, the direction of motion is tangential to the surface at points on the left and right sides of the case. Tangential wavelike surface motions have been shown to be particularly efficient at causing locomotion at low Reynolds number [8, 12]. A sphere that oscillates both radially and moving back and forth along a particular axis excites larger streaming motions than if executing one of these motions alone [27].

At a single moment in time the motor case moves in a single direction. As the internal flywheel rotates, the velocity vector of the case rotates. Induced surface velocities and displacements are axisymmetric in the sense that the displacements and velocities at one time are identical to those at another time after performing a rotation about the center of mass and shifting the phase of oscillation. We have ignored the location of the power wires. Because of the rotational symmetry of the case/fluid boundary, the total momentum imparted to the fluid should average to zero, though the total torque exerted on the fluid might not average to zero. If neutrally buoyant, hence without foam rubber, the object could not swim, though the motor case could rotate.

The vibrational motor is denser than water or glycerin so alone it sinks. Foam rubber, sponge neoprene stripping with adhesive backing, used for weather stripping, was used both to break the rotational symmetry and to make it neutrally buoyant (in glycerin). We attached the foam rubber to the curved rim of the vibrational motor case with double sided tape near the power wires. The rubber foam pad is about the same width as the vibrational motor so that when viewed edge-on the entire body (motor + rubber) is about the same width (~ 3 mm). We started with a rectangular piece of rubber and then trimmed it to achieve neutrally buoyancy. A cartoon of the neutrally buoyant swimmer is shown in Fig. 2 and color photos of it are shown below (see Fig. 4). The buoyancy of the foam rubber also prevents the motor case from rotating.

The vibrational motor swimmer was placed in glycerin (99.7% pure vegetable food grade anhydrous glycerin) in which we mixed some fine blue sand. Mixing the sand also introduced some air bubbles. The air bubbles and fine sand particles served as tracers for the fluid motion. We filmed the swimmer using a 1 Nikon model V1 camera with a 1 Nikkor VR 10–30 mm f/3.5–5.6 lens. Frames from a movie are shown in Figs. 3–7 and the movie itself is available for view at <https://youtu.be/OnP2Mgza0yU>. Each movie frame has 1280×720 pixels and there are 56.48 frames per second. The movie shows that the vibrational motor swims through the glycerin at a rate of 1 body length in about 3 seconds. We filmed the moving vibrational motor in a container with interior 8.25×13.5 cm filled to a height of 6.5 cm with glycerin. We checked that the motor swam at the same speed in a container twice as larger in all dimensions to ensure that we don't mis-interpret boundary affects. We also checked that the motor swam in clean glycerin lacking sand or air-bubbles.

When used for haptic feedback, usually the flat side of the coin vibrational motor is bonded to a surface that is meant to be touched or held. We could achieve neutral buoyancy with the foam rubber fixed to a flat face of the motor case. However we found that swim speed is maximized by sticking the foam rubber to the motor's curved rim rather than the flat face. We infer that breaking the rotational symmetry is important for efficient locomotion in glycerin. The simplest mechanical locomotors have a single degree of freedom for motion, but can move if symmetry between forward and backwards strokes is broken. For example, locomotion is achieved on a table top using a velocity dependent stroke for two masses connected by an actuator with asymmetric friction [29, 47] and with a single hinged microswimmer in a non-Newtonian fluid [34]. For our vibrational motor, points

on the case do not move along a line segment but in a loop, and the rotational symmetry of the motion prevents locomotion unless this symmetry is broken.

Rubber foam behaves visco-elastically and damps vibrations. The rubber foam displaces fluid that could have been moving including near the motor surface where fluid motions are induced. The rotational symmetry of the motion is broken as both of these effects occur on only one side of the motor.

Some notes may be helpful for the reader attempting to build a similar swimmer: The vibrational motor cases are not designed to be impermeable to liquids. If left unpowered in the glycerin for a few hours, when turned on later they rotate less quickly than stop working. They are not meant for continuous operation (cell phone buzzes are short) and so can only run continuously for an hour or two before they wear out. A closed-cell rubber foam, preventing absorption of fluid, is superior as the device would maintain a constant buoyancy. Vibrational motors can be powered autonomously with a pair of 1.5V silver-oxide coin batteries but not with coin lithium cells.

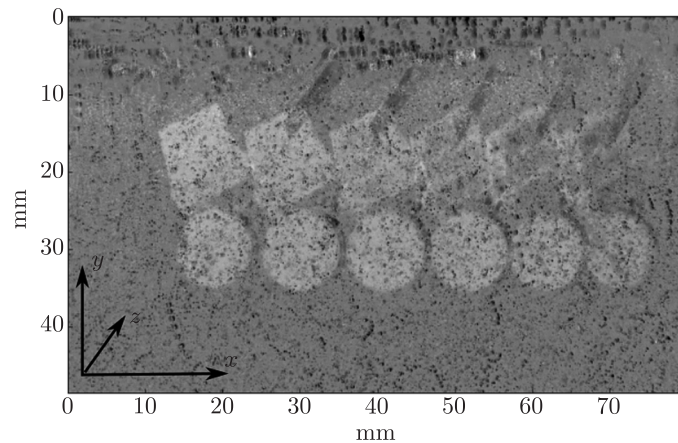


Fig. 3. Six movie frames, each separated by 3.2 seconds, were added after median subtraction. This shows that the vibrational motor moved a body length every 3.2 seconds. The graininess is due to sand and air bubbles that we used to track fluid motion. The vibrational motor is moving to the right. Coordinate axes are shown for describing the motor case oscillations (Eq. (2.1)).

2.1. Swim Speed, Amplitude of Motion and Dimensionless Quantities

When powered, the vibrational motor causes motion in the fluid and the vibrational motor swims steadily through the glycerin. Frames from the movie were extracted using a command-line version of FFmpeg. FFmpeg, <http://ffmpeg.org/>, is a free software project that produces libraries and programs for handling multimedia data. By extracting frames separated by different time intervals we measured the swim speed. Using the standard `scipy` Python software package, we converted six images images, each separated by 3.2 seconds, to grayscale and combined them together computing a median of the values from each frame at each pixel location. We subtracted the median image from each image and then added the six together. The result is shown in Fig. 3 and illustrates the steady swim speed caused by the vibrational motor. The swim speed is 1 body length (using the motor diameter of 10 mm) in 3.2 seconds, equivalent to a velocity of $V_{swim} \approx 3.1 \text{ mm/s}$.

Glycerin (Glycerol) has a viscosity of $\mu = 1.412 \text{ Pa}\cdot\text{s}$ [39] and a density $\rho = 1.261 \text{ g}\cdot\text{cm}^{-3}$ corresponding to a kinematic viscosity of

$$\nu = \frac{\mu}{\rho} = 1.12 \times 10^{-3} \text{ m}^2\text{s}^{-1} = 1.12 \times 10^3 \text{ mm}^2\text{s}^{-1}.$$

Taking a length scale equal to the diameter of the vibrational motor, $D = 10\text{mm}$, and the swim velocity $V_{swim} = 3.1 \text{ mm/s}$ we compute the Reynolds number of the swim motion

$$Re_{swim} = \frac{DV_{swim}}{\nu} = 0.027.$$

The swim Reynolds number Re_{swim} can be compared to that of other swimming organisms or mechanisms. The low Reynolds number implies that the vibrational motor, moving through

Table 1. Properties of the vibrational motor swimming in glycerin

Radius of motor	R	5 mm
Motor width	w	2.5 mm
Vibrational motor frequency	f	10000 rpm
Vibrational motor angular frequency	ω	1050 s ⁻¹
Amplitude of motor case oscillations	A	0.25 mm
Speed of oscillatory case motions	U_0	262.5 mm/s
Kinematic viscosity of glycerin	ν	1.12×10^3 mm s ⁻¹
Viscous diffusion length	l_d	1.46 mm
Swim speed	V_{swim}	3.1 mm/s
Swim Reynolds number	Re_{swim}	0.027
Strouhal number	St	20
Reynolds number	Re	1.2
Streaming Reynolds number	Re_s	0.06
Frequency parameter	β	25

glycerin, is in a regime similar to bacterial motility. However, this Reynolds number ignores the amplitude and frequency of motor motions.

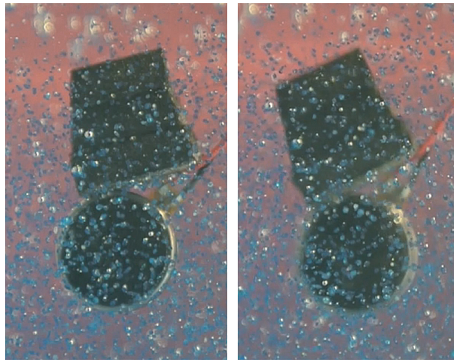


Fig. 4. Regions of two movie frames. The photo on the left was taken when the motor is off. The one on the right is when the motor is on. The edges of the vibrational motor on the right appear blurred because of the motor case oscillations. We use the thickness of the bright rim of the vibrational motor to estimate the amplitude of oscillation. The motor is orientated at a different angle, from vertical in the right image compared to that on the left. The difference in orientation angle is from the torque on the motor caused by the rotational fluid motion. The buoyancy of the foam rubber prevents the motor from rotating.

In Fig. 4 we show regions from two movie frames. The one on the left shows the vibrational motor at rest, before the motor is turned on. The one on the right shows the vibrational motor while it is on and is swimming. The motor is blurred on the right due to the case oscillations. We measured the width of the right edge of the motor in the two frames, finding that it is 4.1 pixels wide for the image on the left and 11.3 pixels wide for the image on the right. We measured the pixel scale, 0.06734 mm/pixel, using the diameter of the motor. The increase in width of the rim is 7.2 pixels and corresponds to a distance of 0.485 mm. Dividing this by two, we estimate the amplitude of surface oscillations,

$$A \approx 0.25 \text{ mm},$$

with an error of about a pixel width or ± 0.07 mm. Orienting a coordinate system with a motor face lying in the x, y plane and z along the line of sight (as viewed in Figs. 1–7, and see Fig. 3 to see the axes), we can describe a point on the case with mean position $\mathbf{x}_0 = (x_0, y_0, z_0)$ and position \mathbf{x} as moving in a circle with

$$\mathbf{x}(t) = \mathbf{x}_0 + A \cos(\omega t) \hat{\mathbf{x}} - A \sin(\omega t) \hat{\mathbf{y}}$$

or with a displacement vector

$$\boldsymbol{\delta} = A \cos(\omega t) \hat{\mathbf{x}} - A \sin(\omega t) \hat{\mathbf{y}} \quad (2.1)$$

that applies to each position on the motor case. Here $\hat{\mathbf{x}}$ is a unit vector in the x direction. The displacement vector also describes the motion of the case/fluid boundary. It is useful to describe the amplitude of motion in units of the vibrational motor's radius, $R = 5\text{mm}$;

$$\epsilon \equiv \frac{A}{R} = 0.05.$$

Using the amplitude we can estimate the velocity of the oscillating case surface

$$U_0 = A\omega = 262.5 \text{ mm/s.}$$

The velocity of oscillation exceeds the swim velocity by a factor about 100.

Vibrating or oscillating objects in a fluid can be described in terms of dimensionless parameters;

$$\text{Strouhal number : } St \equiv R\omega/U_0 = R/A = \epsilon^{-1} = 20$$

$$\text{Reynolds number : } Re \equiv U_0 R/\nu = A\omega R/\nu = 1.2,$$

(e.g., following [19, 35]). Combining these two parameters we compute a parameter called the streaming Reynolds number [4, 35],

$$\text{Streaming Reynolds number : } Re_s \equiv Re St^{-1} = Re \epsilon = \frac{U_0^2}{\omega\nu} = 0.06.$$

The two parameters can also be combined into a frequency parameter, β , (e.g., Section 6.15; [32]), sometimes called the oscillatory Reynolds number, or a frequency Reynolds number ([6]),

$$\text{Frequency parameter : } \beta \equiv Re St = Re/\epsilon = \frac{R^2\omega}{\nu} = 23.4.$$

Important for both time dependent Stokes flow and oscillating boundary layer problems is the viscous diffusion length scale

$$l_d \equiv \sqrt{\frac{2\nu}{\omega}} = 1.46 \text{ mm.}$$

Fluid oscillations are expected to exponentially decay on this length scale [38]. The ratio $A/l_d = \sqrt{Re_s/2}$, so the condition that the amplitude of motion is smaller than the diffusion length, $A \ll l_d$, is equivalent to streaming Reynolds number $Re_s \ll 1$.

The properties and dimensionless parameters of the vibrational motor swimming in glycerin are summarized in Table 1.

2.2. Fluid Motion and Particle Trajectories

Using six frames separated by 0.2 seconds we constructed a median image and again summed median subtracted frames. The result is shown in Fig. 5. Sand particles and air bubbles embedded in the glycerin moved during the 1.2 second interval and they appear in this figure as streaks. Each streak is made by a single particle and comprised of six particle positions. For sand particle diameter 0.2 mm, a velocity of 8 mm/s and kinematic viscosity of glycerin, the Stokes number is $\sim 10^{-4}$ and low enough that the sand particles closely follow fluid streamlines. The black bar on the upper right is from a piece of transparent tape we used to insulate the electrical connections from each other. Flow in the fluid is rotational around the vibrational motor. The rotational streaming

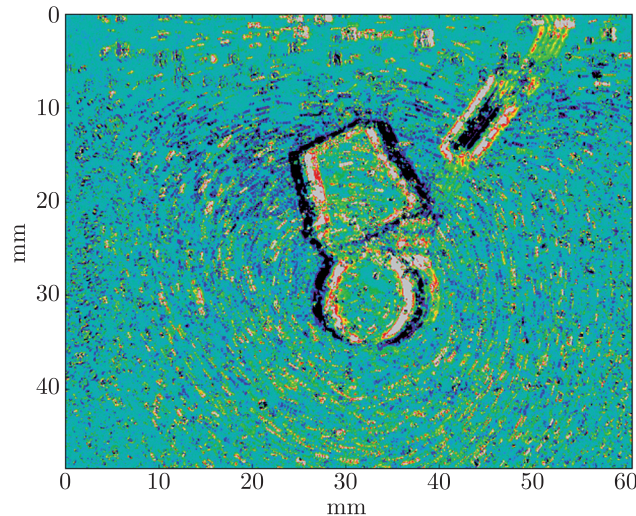


Fig. 5. Six movie frames each separated by 0.2 second were added after median subtraction. Each streak is comprised of about six particle positions for a single particle. The streaks are not due to vibrations from the motor but rather show motions or particles and air bubbles embedded in the glycerin. The rainbow color map was chosen to show the streaks. The black bar on the upper right is from a piece of transparent tape we used to insulate the electrical connections from each other. Flow in the fluid is primarily rotational around the vibrational motor.

lies well outside the width l_d for an oscillating boundary layer, implying that what we are seeing is steady streaming induced by the oscillation near the motor surface.

Figure 4 shows that the foam rubber is tilted (to the left) when the motor is on (photo on the right) compared to its angle when the motor is off (photo on the left). The rotation in the fluid implies that there is a torque on the motor. Because it is more buoyant than the motor, the rubber foam remains on top of the case. The buoyancy force and motor weight counteract the torque on the motor, explaining why it is tilted when the motor is on. The wires also prevent rotation.

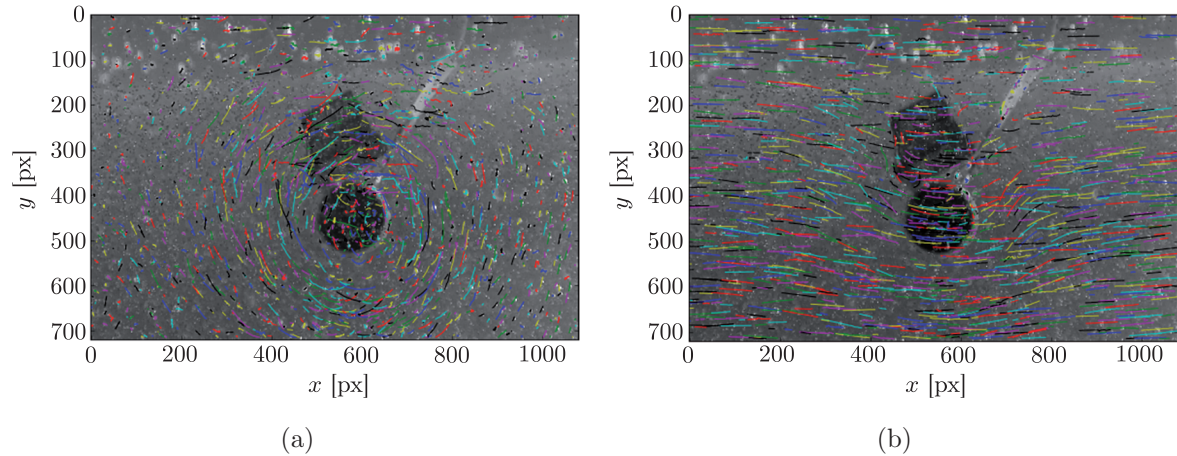


Fig. 6. a) Particle trajectories in the lab reference frame are shown over a 3.5 s time interval with background image showing a movie fame from mid-interval. Particle trajectories are primarily concentric around the motor, showing circulation. Particle motion is clockwise. b) Particle trajectories in the frame of the moving motor are shown over a 1.5 s time interval with background image showing a movie fame from mid-interval. Particles in front of the motor (the right side) are pushed down, under and around the back side of the motor. The white rectangle on the wire is a piece of transparent tape we used to insulate the wire connections from each other.

We used the soft-matter particle tracking software package `trackpy` [1] to identify and track the air bubbles and blue sand particles that are present in the glycerin and seen in the video frames. `Trackpy` is a software package for finding blob-like features in video, tracking them through

time, and analyzing their trajectories. It implements and extends the widely-used Crocker-Grier algorithm [7] in Python. Particles or air bubbles are identified as peaks in the grayscale image frames. Their positions were then tracked through 70 image frames, each separated in time by 0.05 second. Trajectories were rejected if particles moved between frames by more than 5 pixels, were lost for more than 3 frames and were not seen in fewer than 5 frames. The resulting trajectories are shown on top of an image mid time interval in Fig. 6a using 3.5 seconds of video. This figure shows particle trajectories in the lab frame. By shifting each frame according to the motor swim velocity we also corrected trajectories for the swim motion of the motor. In Fig. 6b we show particle trajectories in the motor frame. In this frame particles are stationary on the front edge of the motor and along the wire implying that we have correctly subtracted the motor swim speed to construct the trajectories. The flow under and around the motor is clearer in this frame.

We argued above that the piece of foam rubber breaks the rotational symmetry, however the flow field in Fig. 6a seems nearly rotationally symmetric about the vibrational motor. When viewing the movie, particles on the upper right are swept downwards under the vibrational motor and left behind it on the left. This flow pattern is more clearly seen with particle trajectories in the motor's frame (see Fig. 6b). Particle motion is reduced near the foam rubber, and is lower above the motor than below it. The rotational streaming motion below the motor is not mirrored by a similar flow above the motor and so the fluid has been predominantly moved from right to left, allowing the motor to advance or swim to the right. The foam rubber breaks the rotational symmetry. The propulsion arises because fluid is streaming to the left below the motor.

Particle deviations between two frames (separated by 0.3 s) were used to construct velocity vectors and these are shown in Fig. 7a. Velocities were estimated using the pixel scale (0.067 mm/pixel) and the time interval between the two frames. By subtracting the motion of the motor we made a similar figure but for velocity vectors in the motor frame; Fig. 7b. These figures allow us to estimate the size of the fluid velocities. Fluid velocities approximately 6 mm/s have been induced in the glycerin, with highest velocities near the motor surface of about 8 mm/s. It is somewhat clearer in the movie that the particle motions are about twice the magnitude of the motor swim speed.

That the flow velocities decay with distance from the motor is evident in Fig. 7a as the arrow lengths decrease with distance from the motor. It is likely that the three dimensional steady velocity field could be described by the sum of two Stokes flow steady singularity solutions, a rotlet and a Stokeslet (a point force dipole) (e.g., see Section 6.6 by [32], [31]). Since the flow is predominantly rotational, the rotlet must be larger. The rotlet speed decays with the square of the distance from the vibrational motor (using Table 6.6.2 by [32]).

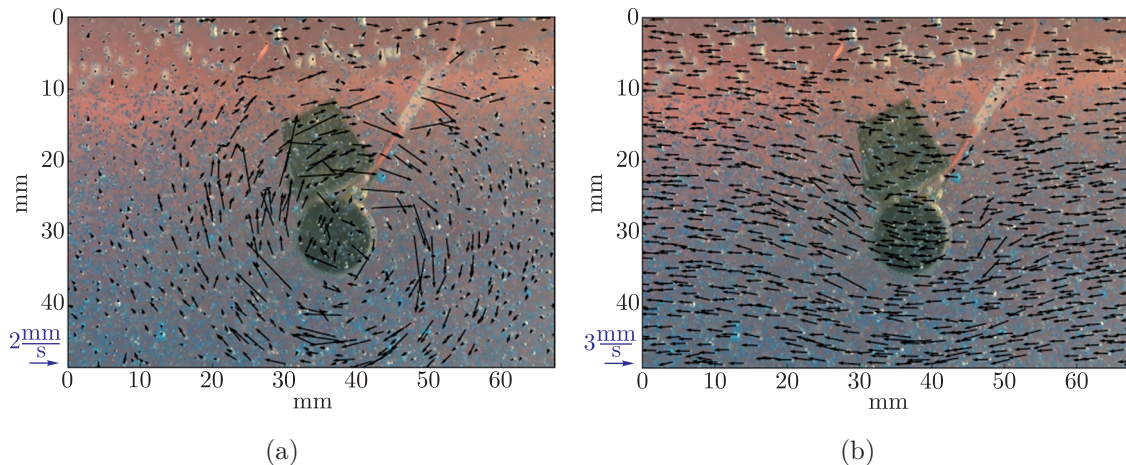


Fig. 7. a) Arrow lengths show particle deviations between two movie frames separated by a 0.3 time interval giving an estimate for particle velocities. Units for arrow length (velocity) are shown in blue on the lower left. Here the velocities are shown in the lab frame. b) Particle velocities are shown in the motor's frame.

3. HYDRODYNAMICS

In the previous section we described the design and construction of a swimmer and measurements of quantities listed in Table 1. The dimensionless parameters the frequency parameter, β , the Reynolds number (computed using the oscillation velocity), Re , the streaming Reynolds number, Re_s , and the Strouhal number, St , (with redundancy between the different parameters), are used to determine which terms in the Navier–Stokes equation must be retained (following [19] chapter 6, also see Section 6.15 by [32] or Section 2 by [35]). We will use the physical sizes R, A, U_0, ω, l_d and ν (motor radius, oscillation amplitude, oscillation velocity, angular frequency, viscous diffusion length and kinematic viscosity) in Section 3.1 to estimate a swim speed derived from the hydrodynamics and compare it to the measured one, V_{swim} . With the measurements of Table 1 in mind, we now discuss hydrodynamic models, first reviewing previous work. Our swimmer is not biologically motivated and previous hydrodynamic explorations are not quite in the right regime. In Section 3.1 we modify the estimate of a steady stream velocity based on an oscillating planar sheet by [43] in the Stokes flow regime. Using the time-dependent or non-stationary Stokes equation we compute the steady streaming velocity induced by the oscillatory motion of a rigid planar sheet. We then use the derived steady streaming velocity to estimate a swim velocity and we compare it to the one we measured from our mechanism in Section 2.1.

[43] considered the swimming velocity of a sheet exhibiting low amplitude traveling waves on its surface. Using global solutions to the Stokes equations, Taylor expanded the boundary displacement and velocity in powers of the wave amplitude and matched expansion coefficients to solve for the fluid motions. He found that the swim velocity (or induced steady streaming velocity in the fluid) is proportional to the square of the surface wave amplitude. [4] estimated swim velocities by computing the velocity field in an oscillating boundary layer in the vicinity of a surface exhibiting low amplitude plane waves. [9] extended Taylor's formalism to more general wavelike solutions motivated by the geometrical or gauge formalism by [40]. Deformations are described in terms of a Fourier basis of vector fields. A swim stroke is a periodic combination of these vector fields that returns the sheet (or body) to its original shape. Curvature coefficients depend on the commutators of these vector fields and the swimming velocity depends on the square of the wave amplitude.

The oscillating boundary layer of a vibrating or oscillating object in a viscous fluid should have height similar to l_d , the viscous diffusion length [4, 26, 30, 42]. However, a steady streaming motion, sometimes called Stokes drift, that extends past the boundary layer, can be induced by the oscillatory flow [4, 27, 35]. The steady streaming flow can be induced even in incompressible flows, so need not be called “acoustic streaming”. The streaming flow does not necessarily arise solely from matching the fluid velocity to a moving boundary (as by [43]). It can be caused by the Reynolds stress or advective term, $\mathbf{u} \cdot \nabla \mathbf{u}$, in the Navier–Stokes equation. Because this term is non-linear and depends on the square of the velocity, the streaming velocity outside the Stokes layer (with width l_d) can depend on the square of the amplitude of the oscillatory motion [27], or $Re_s^{1/2}$ [35], depending on the shape and dimension of the vibrating or oscillating object and the streaming Reynolds and Strouhal numbers.

The *Tangent Plane Approximation* [4, 9] assigns a flow velocity to each region of the surface based on expansion of the surface deformation in terms of plane wave motions. For a slender body such as a flagellum for which the radius of curvature is larger compared to the diameter of the filament, a related approximation is known as “Resistive Force Theory” [13]. This approximation postulates that each infinitesimal segment is hydrodynamically uncoupled from the others and that the drag forces associated with normal and tangential motions are approximately proportional to the local filament velocity, with local drag coefficients those of a straight cylinder.

The tangent plane approximation computes local streaming velocities across the surface of the motor and then sums these velocities to estimate the swim velocity of a body. With the goal of using such a local approximation on the vibrational motor, we consider streaming caused by the oscillatory motion of a rigid planar sheet.

3.1. Circular Oscillation of a Planar Sheet

We look for a solution to the equations describing the fluid that are consistent with a rigid but moving sheet boundary. The motion of the vibrational motor differs from the short wavelength (compared to body diameter) and traveling wave surface deformations considered by previous

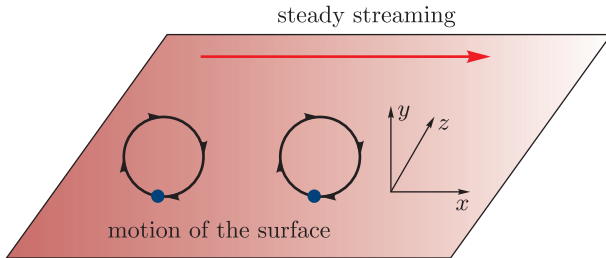


Fig. 8. Illustrating the oscillation for the planar sheet. Every point in the plane moves in a loop in x and y directions. Every point moves in the same trajectory shape simultaneously. Here y is normal to the plane and the x and z directions lie in the plane. Each point on the plane has motion similar to every other point, so fluid motions induced by the boundary motion should be independent of x and z . The fluid is present in the infinite half-plane covering $y > 0$ and at negative y during half the oscillation.

studies [4, 9, 43]. For our study the surface is rigid, whereas for theirs the surface deforms. We look at a sheet with each point undergoing the same periodic motion; see Fig. 8 for an illustration. The surface moves in x and y with the x axis parallel to the sheet and the y axis normal to it. We neglect z (also in the sheet plane) as there is no motion in that direction. We use the infinite half-plane covering $y > 0$.

We work in units of distance divided by the radius R , time in units of ω^{-1} and velocities in units of $U_0 = A\omega$ (following [19] chapter 6, also see Section 6.15 by [32]). We choose this scaling because we are interested in the fluid flow at distances of R rather than at distances of A , the amplitude of oscillation. The surface displacement vector

$$\delta(x, t) = \epsilon(\cos t \hat{\mathbf{x}} - \sin t \hat{\mathbf{y}}) \quad (3.1)$$

where $\epsilon = A/R$ and we have omitted functional dependence on z in the plane. The velocity on the boundary is

$$\mathbf{V}_{\text{boundary}}(x, t) = -\sin t \hat{\mathbf{x}} - \cos t \hat{\mathbf{y}}. \quad (3.2)$$

Both are independent of mean x value, and the mean position of the moving planar surface is at $y = 0$. The time derivative of displacement δ is equal to that of the velocity on the boundary after dividing by U_0 .

The velocity in the fluid has components $\mathbf{u}(y, t) = u\hat{\mathbf{x}} + v\hat{\mathbf{y}}$. As the motion of points in the sheet is independent of x , the fluid velocity should be independent of x . For a no-slip boundary the velocity of a fluid element near the surface should match that of the surface. Using a Taylor expansion

$$\mathbf{V}_{\text{boundary}} = \mathbf{u}|_{y=0} + (\delta(t) \cdot \nabla) \mathbf{u}|_{y=0} + \dots \quad (3.3)$$

Using the y -component of the displacement (Eq. (3.1)), the x -component of Eq. (3.3) becomes

$$-\sin t = u|_{y=0} - \epsilon \sin t \frac{\partial u}{\partial y} \Big|_{y=0} \quad (3.4)$$

to first order in ϵ . Because of our choice of units, and because $\epsilon < 1$ for the vibrational motor, we can expand the boundary condition in orders of ϵ .

Equation (3.3) relating the fluid flow to the boundary motion is equivalent to Eq. (5) by [4] and the commutator of two velocity vector fields shown with Eq. (2.19) by [9]. The geometric paradigm is that surface motions transverse to the plane do not commute with motions normal to the plane.

The Navier–Stokes equation

$$\frac{\partial \mathbf{u}'}{\partial t'} + (\mathbf{u}' \cdot \nabla') \mathbf{u}' = -\frac{\nabla p}{\rho} + \nu \nabla'^2 \mathbf{u}'$$

for velocity \mathbf{u}' , time t' and $\nabla' = \frac{\partial}{\partial \mathbf{x}'}$. Using our rescaled variables ($\mathbf{x} = \mathbf{x}'/R$, $t = \omega t'$, $\mathbf{u} = \mathbf{u}'/U_0$), the Navier–Stokes equation

$$\frac{\partial \mathbf{u}}{\partial t} + \epsilon(\mathbf{u} \cdot \nabla) \mathbf{u} = -\frac{\nabla p}{U_0^2 \rho} + \beta^{-1} \nabla^2 \mathbf{u}.$$

For our problem $\epsilon \sim \beta^{-1}$ because the Reynolds number $Re \sim 1$. In the low Reynolds number limit the smallest term is the second one on the left ($\propto \mathbf{u} \cdot \nabla \mathbf{u}$) and it can be ignored, giving the non-stationary Stokes flow problem or linearized Navier–Stokes equation. We do this here, but keep in mind that this is a poor approximation for our vibrational motor. If our motor were in a somewhat higher viscosity fluid, it would be a decent approximation. Focusing on the x-component of velocity and dropping the non-linear term

$$\frac{\partial u}{\partial t} = \beta^{-1} \frac{\partial^2 u}{\partial y^2}. \quad (3.5)$$

We have neglected the pressure term because of the x translational symmetry.

Equation (3.5) is a heat equation with solution

$$u(s) = ae^{-k_s y} \cos(k_s y - st) + be^{-k_s y} \sin(k_s y - st) \quad (3.6)$$

with $k_s = \sqrt{\frac{s\beta}{2}}$ and constant coefficients a, b . We have restricted this solution so that it remains finite at large positive y . The general solution is a sum or integral over frequencies s . Note that the zero frequency solution does not decay with y . We consider a total solution that is a sum of a constant term ($s = 0$), a term with frequency $s = 1$, and a term with frequency $s = 2$, each with unknown coefficients. We insert this into our boundary condition (Eq. (3.4)) and solve for the coefficients, finding

$$u(y, t) \approx e^{-k_1 y} \sin(k_1 y - t) + \frac{\epsilon k_1}{2} - \frac{\epsilon k_1}{2} e^{-k_2 y} \sqrt{2} \sin(k_2 y - 2t + \pi/4)$$

to first order in ϵ . Here $k_1 = \sqrt{\beta/2}$ and $k_2 = \sqrt{\beta}$. The constant term is the streaming velocity

$$u_s = \frac{\epsilon k_1}{2} = \epsilon \sqrt{\beta/8} = \sqrt{Re_s/8}. \quad (3.7)$$

The steady streaming velocity is in the same direction as the motion of the surface at largest y from the mean, (at $t = 3\pi/2$ in Eqs. (3.1), (3.2)) and as shown with a long arrow in Fig. 8. The dependence of the streaming speed on $\sqrt{Re_s}$ has been seen previously in oscillating flows near a surface (see Section 2.4 by [35]). In the limit of high viscosity $u_s \rightarrow 0$, the streaming velocity vanishes, and the vibrational motor would not swim.

In plane wave studies in the Stokes flow limit [4, 9, 43], the fluid flow also decays exponentially away from the surface, but there the exponential decay length of the flow is set by the wavelength of surface perturbations rather than the frequency of the motion and the viscous diffusion length at that frequency.

Restoring units to Eq. (3.7)

$$\begin{aligned} V_{stream} &\approx U_0 \sqrt{\frac{Re_s}{8}} = \frac{U_0}{2} A \sqrt{\frac{\omega}{2\nu}} \\ &= \frac{U_0 A}{2 l_d} = \frac{A\omega}{2} \frac{A}{l_d}. \end{aligned} \quad (3.8)$$

The streaming velocity can be written so that it is independent of radius R , consistent with the planar approximation.

Evaluating the streaming speed (Eq. (3.8)) for the amplitude, frequency and viscosity of the vibrational motor in glycerin (using values listed in Table 1) we find

$$V_{stream} \sim 22 \text{ mm/s}. \quad (3.9)$$

This exceeds the streaming motions we measured from particle velocities in Figs. 7 by a factor of 3. We considered planar flow and the vibrational motor is only 2.5 mm wide. A better model would take into account the width of the motor case and an associated drag force. We approximated the flow using unsteady or non-stationary Stokes flow, however the Reynolds number, $Re \sim 1$, is not sufficiently low to make this approximation a good one. The inaccuracy of these two approximations may account for the difference between the streaming velocity estimated with Eq. (3.9) and that we

measured. The steady ($s = 0$) solution to the planar problem (Eq. (3.6)) is independent of distance from the surface. A three dimensional model could approximate the steady flow as the sum of two steady singularity solutions, a rotlet and a Stokeslet (e.g., see Section 6.6 by [32], [31]) with both flows decaying as a function of distance from the center of the vibrational motor.

In the second line of Eq. (3.8) we see that the streaming velocity depends on the square of the displacement amplitude, as expected for a second order effect. In the low frequency limit, the streaming velocity predicted using Stokes flow is $V_{\text{swim}} \sim \epsilon_\lambda^2 c$ [9, 43], where c is the speed of surface waves and $\epsilon_\lambda = A/\lambda$ is the ratio of oscillation amplitude to wavelength. Using the time dependent Stokes equations (as done here) we find a dependence on the viscous diffusion length scale that arises because the exponential decay of the oscillating flow depends on this scale. In contrast in the low frequency limit, the exponential decay follows from the solution of Laplace's equation and depends on the wavelength of the planar perturbations. A planar model that solves the time dependent Stokes equations for plane waves should give a solution that is consistent with both results.

Adopting the approach of the tangent plane approximation we can integrate the streaming velocities over the motor surface, (see Eq. (3.1) by [9] and associated discussion) to estimate a swim velocity. Velocities in front of and behind the motor are opposite and in the vertical direction. The vertical components don't contribute to the horizontal swim velocity. The velocity below the motor is unimpeded by the rubber foam and so can be estimated from Eq. (3.9). The motor does *not* get an opposite push from its top, because the softness and porosity of the foam rubber relaxes the boundary condition (Eq. (3.3)) and reduces the speed of the streaming motion on that side of the motor. The streaming motion on the top of the motor we can consider to be zero. Weighting by area and using these 4 values, the swim speed is about 1/4 of the streaming velocity. We would estimate a swim speed of a few mm/s and in the direction counter to the flow below the motor. This is consistent with the swim speed of the motor and suggests that Eq. (3.8) is correct to order of magnitude.

Neutral buoyancy can be achieved with a light rigid body. But if firmly attached to the vibrational motor it too would vibrate and so induce steady streaming in the fluid. If the rubber foam were replaced with a solid but rigid and light body, the device would not swim because induced streaming above the motor would counteract the induced streaming below the motor. The foam rubber must absorb or damp vibrations on one side of the motor so that it will swim.

Most estimates of swimming velocity work in the limit of small wavelength surface motions (wavelength smaller than the object diameter, e.g., [31]) — with swim velocities dependent on the wavelength (for example Eq. (36) by [4]). Here we estimated a swim speed for a solid body motion that depends only on the velocity of surface motion, frequency and fluid viscosity (Eq. (3.8)). The streaming motion is induced by the non-linearity of the surface boundary condition (as studied by [4, 9, 43]) rather than the advective or nonlinear term [26] because we have neglected the non-linear term in the Navier–Stokes equation.

Equation (3.8) suggests that the swim velocity can be maximized by increasing the amplitude of oscillation, A , the angular frequency of internal rotation ω and decreasing the viscosity. This pushes the solution to higher Reynolds number, $Re > 1$, where the advective or non-linear term in the Navier–Stokes equation cannot be neglected. In this regime steady streaming is still present but the flow can be more complex [6, 17, 21] and perhaps experimental observations or simulations are required to understand the flow field and resulting swim velocity.

We have assumed that the vibrational motion of the motor (Eqs. (2.1), (3.1)) is circular. However the amplitude of case oscillation depends on the motor recoil and how the fluid and rubber foam oppose it. The surface displacement is more generally an ellipse.

For the planar model with $\hat{\mathbf{x}}$ tangent to the surface and $\hat{\mathbf{y}}$ normal to it, we can modify Eq. (3.1) to describe elliptical motion; $\delta = \epsilon \cos t \hat{\mathbf{x}} - \epsilon \gamma \sin t \hat{\mathbf{y}}$. The ratio of y to x amplitudes is γ and $\gamma \sim 1$ for nearly circular motion. Here the amplitude of motion normal to the surface is proportional to γ and the variables are scaled to the displacement and velocity in the direction parallel to the surface. The boundary condition (Eq. (3.4)) and solution (Eq. (3.6)) to the non-stationary Stokes equation give streaming velocity the same as before (Eq. (3.8)) but multiplied by γ . The streaming speed (including units),

$$V_{\text{stream}} \approx \frac{A\omega}{2} \frac{A\gamma}{l_d},$$

shows the dependence on the tangential and normal amplitudes of motion, consistent with the geometric interpretation that the two motions do not commute. The tangent plane approximation can again be used to estimate the streaming motions on different sides of the motor but taking into account how the ratio of amplitudes, γ , depends on the local angle of the motor surface. The blur in our movie frames when the motor is on is consistent with nearly circular motion, $\gamma \sim 1$, so we do not modify our rough estimate for the swim velocity.

4. SUMMARY AND DISCUSSION

We succeeded in getting a 1 cm diameter coin vibration motor to swim in glycerin at 3 mm/s by breaking its rotational symmetry of motion. Symmetry was broken using a piece of foam rubber that also served to give the motor neutral buoyancy and prevent it from rotating. Movies of the motor swimming in glycerin with sand and bubble tracers illustrate that rotational steady streaming motions are induced by the motor and that the asymmetry in distribution of these motions is consistent with propulsion. The swimming vibrational motor represents a low-cost realization of the concepts for swimming by internal motions previously proposed and discussed by [6, 9, 44]. Using the swim velocity to compute the Reynolds number, we find that it is low, $Re_{swim} \sim 0.03$, and in the regime of bacterial motility. As bacteria don't vibrate, this concept for locomotion is not helpful for understanding bacterial locomotion. However, our swimmer is novel and inexpensive, so may inspire development of small robotic swimmers that are robust because they have no external moving parts.

Most previous works either focused on acoustically driven streaming due to oscillatory flows [30, 35, 42] or short wavelength surface waves in the time independent (or stationary) Stokes regime to estimate swim speeds of periodically deforming bodies [4, 9, 31, 40, 43]. We used a translationally invariant oscillating planar motion model and non-stationary Stokes flow to estimate a steady streaming velocity. We find that steady streaming, extending past an oscillating boundary layer, arises from a second order effect induced by the moving boundary, rather than by Reynolds stress (or advective non-linear term) as is possible in many acoustic streaming problems. Because the oscillating flow decays exponentially with the viscous diffusion length scale, the steady streaming velocity is also sensitive to this scale. Using the tangent plane approximation, this planar problem suggests that the swim velocity should be a factor a few smaller than

$$V_{swim} \sim A\omega\sqrt{Re_s/8},$$

where a correction factor (multiplying the above estimate) depends on a sum of the steady streaming motions induced on different sides of the body. This relation is appropriate for Reynolds number $Re = U_0/(R\nu) < 1$ where $U_0 = A\omega$ is the velocity of motor case oscillation.

The amplitude of motion, A , vibrational velocity, U_0 , and ellipticity of motion, depend on the force exerted on the motor by the fluid as well as the distance between motor centroid and center of mass, d_m . Defining a parameter $\alpha = d_m/R$ (Eq. (2.4) by [6]), [6] used numerical simulations to estimate the amplitude of motion for a linear rather than rotational shifting internal mass distribution. Their result is given in their Eq. (2.18) and is approximately consistent with $A/R \sim \frac{\alpha}{2+\beta-1}$ giving $A \sim d_m/2$ for our frequency parameter $\beta \sim 25$. The amplitude A would need to be measured or computed to estimate swim velocities for different frequency vibrational motors in different fluids. For $\beta > 1$ and $Re \lesssim 1$, Eq. (3.8) and the scaling by [6] suggest that the swim velocity $V_{swim} \sim \alpha^2(R/l_d)R\omega/8$.

Use of the non-stationary Stokes equation allowed us to estimate the streaming velocity caused by a rigid but oscillating surface and is not limited to short wavelength surface perturbations (as was true for the Stokes regime studies by [4, 9, 31, 43]). However the non-stationary Stokes equation neglects the advective term in the Navier–Stokes equation and this term should not be neglected at $Re \gtrsim 1$. Steady streaming is predicted at this [37] and higher Reynolds numbers where the dynamics may become increasingly complex (e.g., [6, 17, 21, 42]). Unfortunately, our swimming vibrational motor, with $Re \sim 1$, is in this regime. Also, our vibrational motor is thin, with width to diameter ratio of 1/4, and the tangent plane approximation is inaccurate. Improved calculations or simulations can improve upon our rough approximations by taking into account the structure of the boundary layer (or layers; [21, 42]) and the three-dimensional structure of the vibrational motor and associated fluid flow (e.g., [6, 44]).

ACKNOWLEDGMENTS

We thank Eric Blackman, Eva Bodman, Dan Tamayo, Luke Okerlund, Logan Meredith and Andrea Kueter-Young for helpful discussions.

REFERENCES

1. Allan, D., Caswell, T., Keim, N., and van der Wel, C., trackpy: Trackpy v0.3.1 [Data set]. Zenodo. <http://doi.org/10.5281/zenodo.55143> (2016).
2. Alexander, R., *Principles of Animal Locomotion*, Princeton, N.J.: Princeton Univ. Press, 2003.
3. Bertelsen, A. F., An Experimental Investigation of High Reynolds Number Steady Streaming Generated by Oscillating Cylinders, *J. Fluid Mech.*, 1974, vol. 64, no. 3, pp. 589–598.
4. Brennen, C., An Oscillating-Boundary-Layer Theory for Ciliary Propulsion, *J. Fluid Mech.*, 1974, vol. 65, no. 4, pp. 799–824.
5. Brennen, C. and Winet, H., Fluid Mechanics of Propulsion by Cilia and Flagella, *Annu. Rev. Fluid Mech.*, 1977, vol. 9, pp. 339–398.
6. Childress, S., Spagnolie, S. E., and Tokieda, T., A Bug on a Raft: Recoil Locomotion in a Viscous Fluid, *J. Fluid Mech.*, 2011, vol. 669, pp. 527–556.
7. Crocker, J. C. and Grier, D. G., Methods of Digital Video Microscopy for Colloidal Studies, *J. Colloid Interface Sci.*, 1996, vol. 179, no. 1, pp. 298–310.
8. Delgado, J. and González-García, J. S., Evaluation of Spherical Shapes Swimming Efficiency at Low Reynolds Number with Applications to Some Biological Problems, *Phys. D*, 2002, vol. 168/169, pp. 365–378.
9. Ehlers, K. M. and Koiller, J., Micro-Swimming without Flagella: Propulsion by Internal Structures, *Regul. Chaotic Dyn.*, 2011, vol. 16, no. 6, pp. 1–30.
10. Ehlers, K. M., Samuel, A. D., Berg, H. C., and Montgomery, R., Do Cyanobacteria Swim Using Traveling Surface Waves?, *Proc. Natl. Acad. Sci. USA*, 1996, vol. 93, pp. 8340–8343.
11. Elgeti, J., Winkler, R. G., and Gompper, G., Physics of Microswimmers — Single Particle Motion and Collective Behavior: A Review, *Rep. Progr. Phys.*, 2015, vol. 78, no. 5, 056601, 50 pp.
12. González-García, J. and Delgado, J., Comparison of Efficiency of Translation between a Deformable Swimmer versus a Rigid Body in a Bounded Fluid Domain: Consequences for Subcellular Transport, *J. Biol. Phys.*, 2006, vol. 32, no. 2, pp. 97–115.
13. Gray, J. and Hancock, G. J., The Propulsion of Sea-Urchin Spermatozoa, *J. Exp. Biol.*, 1955, vol. 32, pp. 802–814.
14. Harman, M., Vig, D. K., Radolf, J. D., and Wolgemuth, C. W., Viscous Dynamics of Lyme Disease and Syphilis Spirochetes Reveal Flagellar Torque and Drag, *Biophys. J.*, 2013, vol. 105, no. 10, pp. 2273–2280.
15. Hogg, T., Using Surface-Motions for Locomotion of Microscopic Robots in Viscous Fluids, *J. Micro-Bio Robotics*, 2014, vol. 9, nos. 3–4, pp. 61–77.
16. Hosoi, A. E. and Goldman, D. I., Beneath Our Feet: Strategies for Locomotion in Granular Media, *Annu. Rev. Fluid Mech.*, 2015, vol. 47, pp. 431–453.
17. Honji, H., Streaked Flow around an Oscillating Circular Cylinder, *J. Fluid Mech.*, 1981, vol. 107, pp. 509–520.
18. Khapalov, A. Y., Micromotions of a Swimmer in the 3-D Incompressible Fluid Governed by the Nonstationary Stokes Equation, *SIAM J. Math. Anal.*, 2013, vol. 45, no. 6, pp. 3360–3381.
19. Kim, S. and Karrila, S. J., *Microhydrodynamics: Principles and Selected Applications*, Boston, Mass.: Butterworth/Heinemann, 1991.
20. Klotsa, D., Baldwin, K. A., Hill, R. J. A., Bowley, R. M., and Swift, M. R., Propulsion of a Two-Sphere Swimmer, *Phys. Rev. Lett.*, 2015, vol. 115, no. 24, 248102, 5 pp.
21. Kotas, Ch. W., Yoda, M., and Rogers, P. H., Visualization of Steady Streaming Near Oscillating Spheroids, *Exp. Fluids*, 2007, vol. 42, no. 1, pp. 111–121.
22. Lauga, E., Life around the Scallop Theorem, *Soft Matter*, 2011, vol. 7, pp. 3060–3065.
23. Lauga, E. and Powers, Th. R., The Hydrodynamics of Swimming Microorganisms, *Rep. Prog. Phys.*, 2009, vol. 72, no. 9, 096601, 58 pp.
24. Lauga, E., Bacterial Hydrodynamics, *Annu. Rev. Fluid Mech.*, 2016, vol. 48, pp. 105–130.
25. Lighthill, M. J., On the Squirming Motion of Nearly Spherical Deformable Bodies through Liquids at Very Small Reynolds Numbers, *Commun. Pure Appl. Math.*, 1952, vol. 5, pp. 109–118.
26. Lighthill, J., Acoustic Streaming, *J. Sound Vibration*, 1978, vol. 61, no. 3, pp. 391–418.
27. Longuet-Higgins, M. S., Viscous Streaming from an Oscillating Spherical Bubble, *R. Soc. Lond. Proc. Ser. A Math. Phys. Eng. Sci.*, 1998, vol. 454, no. 1970, pp. 725–742.
28. Nadal, F. and Lauga, E., Asymmetric Steady Streaming As a Mechanism for Acoustic Propulsion of Rigid Bodies, *Phys. Fluids*, 2014, vol. 26, no. 8, 082001, 26 pp.

29. Noselli, G. and DeSimone, A., A Robotic Crawler Exploiting Directional Frictional Interactions: Experiments, Numerics, and Derivation of a Reduced Model, *R. Soc. Lond. Proc. Ser. A Math. Phys. Eng. Sci.*, 2014, vol. 470, no. 2171, 20140333, 15 pp.
30. Nyborg, W. L., Acoustic Streaming near a Boundary, *J. Acoust. Soc. Am.*, 1958, vol. 30, no. 4, pp. 329–339.
31. Pedley, T. J., Brumley, D. R., and Goldstein, R. E., Squirmers with Swirl: A Model for Volvox Swimming, *J. Fluid Mech.*, 2016, vol. 798, pp. 165–186.
32. Pozrikidis, C., *Introduction to Theoretical and Computational Fluid Dynamics*, 2nd ed., New York: Oxford Univ. Press, 2011.
33. Purcell, E. M., Life at Low Reynolds Number, *Am. J. Phys.*, 1977, vol. 45, no. 1, pp. 3–11.
34. Qiu, T., Lee, T.-C., Mark, A. G., Morozov, K. I., Münster, R., Mierka, O., Turek, S., Leshansky, A. M., and Fischer, P., Swimming by Reciprocal Motion at Low Reynolds Number, *Nat. Commun.*, 2014, vol. 5, 5119, 38 pp.
35. Riley, N., Steady Streaming, *Annu. Rev. Fluid Mech.*, 2001, vol. 33, pp. 43–65.
36. Saffman, P. G., The Self-Propulsion of a Deformable Body in a Perfect Fluid, *J. Fluid Mech.*, 1967, vol. 28, no. 2, pp. 385–389.
37. Sadiq, M. A., Steady Flow Produced by the Vibration of a Sphere in an Infinite Viscous Incompressible Fluid, *J. Phys. Soc. Jpn.*, 2011, vol. 80, 094403, 6 pp.
38. Schlichting, H., Berechnung ebner periodischer Grenzschichtströmungen, *Phys. Z.*, 1932, vol. 33, pp. 327–335.
39. Segur, J. B. and Oberstar, H. E., Viscosity of Glycerol and Its Aqueous Solutions, *Ind. Eng. Chem.*, 1951, vol. 43, no. 9, pp. 2117–2120.
40. Shapere, A. and Wilczek, F., Geometry of Self-Propulsion at Low Reynolds Number, *J. Fluid Mech.*, 1989, vol. 198, pp. 557–685.
41. Stone, H. A. and Samuel, A. D. T., Propulsion of Microorganisms by Surface Distortions, *Phys. Rev. Lett.*, 1996, vol. 77, no. 19, pp. 4102–4104.
42. Stuart, J. T., Double Boundary Layers in Oscillatory Viscous Flow, *J. Fluid Mech.*, 1966, vol. 24, no. 4, pp. 673–687.
43. Taylor, G. I., Analysis of the Swimming of Microscopic Organisms, *Proc. R. Soc. Lond. Ser. A Math. Phys. Eng. Sci.*, 1951, vol. 209, no. 1099, pp. 447–461.
44. Vetchanin, E. V., Mamaev, I. S., and Tenenev, V. A., The Self-Propulsion of a Body with Moving Internal Masses in a Viscous Fluid, *Regul. Chaotic Dyn.*, 2013, vol. 18, no. 1, pp. 100–117.
45. Vetchanin, E. V. and Kilin, A. A., Control of Body Motion in an Ideal Fluid Using the Internal Mass and the Rotor in the Presence of Circulation around the Body, *J. Dyn. Control Syst.*, 2017 (to appear).
46. Vladimirov, V. A., Dumbbell Micro-Robot Driven by Flow Oscillations, *J. Fluid Mech.*, 2013, vol. 717, R8, 11 pp.
47. Wagner, G. L. and Lauga, E., Crawling Scallop: Friction-Based Locomotion with One Degree of Freedom, *J. Theor. Biol.*, 2013, vol. 324, pp. 42–51.